International Journal of Ocean System Engineering 2(2) (2012) 82-91
DOI 10.5574/IJOSE.2011.2.2.082

Numerical Simulation of Welding Residual Stress Distribution on T-joint Fillet Structure

Se-Yun Hwang[1], Jang-Hyun Lee[1*], Sung-Chan Kim[2] and Kodakkal Kannan Viswanathan[3]

[1]*Department of Naval Architecture and Ocean Engineering, Inha University, Incheon 402-751, Korea*

[2]*Department of Naval Architecture and Ocean Engineering, Inha Technical College, Incheon 402-751, Korea*

[3]*Department of Department of Mathematics, Faculty of Science, Universiti Teknologi Malaysia, 81310 Skudai, Johor, Malaysia*

(Manuscript Received February 20, 2012; Revised March 20; 2012; Accepted May 20, 2012)

Abstract

Fillet welding is widely used in the assembly of ships and offshore structures. The T-joint configuration is frequently reported to experience fatigue damage when a marine structure meets extreme loads such as storm loads. Fatigue damage is affected by the magnitude of residual stresses on the weld. Recently, many shipping registers and design guides have required that the fatigue strength assessment procedure of seagoing structures under wave-induced random loading and storm loading be compensated based on the effect of residual stresses. We propose a computational procedure to analyze the residual stresses in a T-joint. Residual stresses are measured by the X-ray diffraction (XRD) method, and a 3-D finite element analysis (FEA) is performed to obtain the residual stress profile in the T-joint. The proposed finite element model is validated by comparing experiments with computational results, and the characteristics of the residual stresses in the T-joint are discussed.

Keywords: Welding, Residual stress, FEA, XRD, T-joint, Storm load.

1. Introduction

Fillet welding have been extensively used in the fabrication of ships and ocean structures. Due to localized heating by the welding process and rapid cooling, residual stresses can occur in and around the welding zone. Though residual stresses are unavoidable in welding, the effects of these stresses on the fatigue strength of welded structures cannot be disregarded. The presence of residual stresses in structures can significantly affect the fatigue behavior during external cyclic loading.

The effect of residual stresses may either be beneficial or detrimental, depending on magnitude, sign and distribution of the stresses with respect to the load-induced stresses. Residual stresses in tension are detrimental and are often in the magnitude of the materials yield strength. The tensile residual stresses will reduce the fatigue life of the structure by increasing the growth of the fatigue crack, while compressive residual stresses will decrease fatigue crack growth rate [1, 2]. Therefore, accurate prediction and reduction of welding residual stress are critical in improving the fatigue strength of welded structures. The initiation and propagation of cracks at a welded joint under cyclic loading is primarily determined by the residual stress distribution while crack initiation is strongly affected by the magnitude of the welding residual stresses. Many studies dealing with the effects of residual stresses on welded structures have shown that the fatigue life and fatigue strength of such structures could be improved by reducing the influence of tensile residual stresses on as-welded components[3, 4, 5].

*Corresponding author. Tel.: +82-32-860-7345, Fax.: +82-32-864-5850.
E-mail address: jh_lee@inha.ac.kr.

Seagoing marine structures are often subjected to dynamic service loads, including random fluctuations of storm loading. Tomita et al. (1995)[6] reported that a significant proportion of fatigue cracks occurring in ship and ocean structures occurred by wave-induced random loading. In high wave height conditions, wave height reaches a maximum value at one point. The higher wave condition is called 'storm condition or loading'. The fatigue behavior of those seagoing structures is complicated by numerous factors intrinsic to the nature of welded joints. Recently, shipping registers and classifications have required that a fatigue life assessment must consider residual stress distributions for a marine vessel that experiences storm loading [7]. It is obvious that a detailed knowledge of the residual stress profiles generated is required together with methods for incorporating these into fatigue lifetime calculation procedures [3, 8]. This requirement is schematically illustrated in Fig. 1.

Estimating the fatigue life of welded joints can be complex, costly, and time consuming due to complex joint geometry, the number of stress concentration points, and the residual stress distributions. Assessment of the fatigue life of welded structures considering residual stresses should be performed using fracture mechanics, and should also be based on residual stresses. Accurate prediction of residual stresses induced by the welding process is very difficult because the thermal and mechanical behavior in welding includes extremely high temperatures, a moving heat source, and the temperature dependence of material properties. Finite element analysis (FEA) of the welding process is effective in predicting residual stresses.

We performs a thermal elastic-plastic analysis using finite element techniques to analyze the thermomechanical behavior and assess residual stresses in T-joint weldment, and also measures the residual stress by a non-destructive method. This study is the preceding task for the prediction of fatigue life in a T-joint fillet, which is the most commonly reported fatigue damage in ships and ocean structures subjected to storm loading. The residual stresses of a T-joint weld specimen were measured using X-Ray diffraction (XRD), and a three-dimensional (3-D) thermal elasto-plastic FEA was performed. The validity of the FEA was demonstrated by comparing FEA results with experiment results.

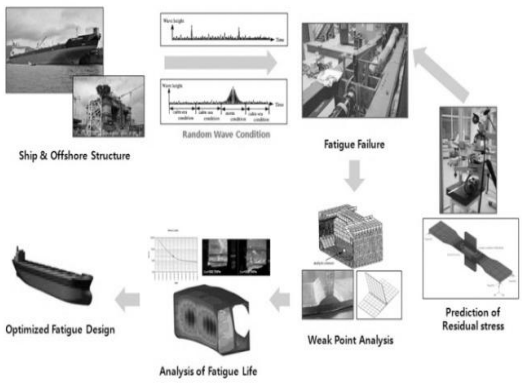

Fig. 1. Fatigue life assessment process

2. Measured Residual Stress

2.1 Specimens

AH32 steel was chosen for this study because it is widely used for marine structures, and it is easily welded without special heat treatment. The welded specimens were fabricated from TMCP (Thermo-Mechanical Control Process) AH32 structural steel. The chemical composition and mechanical properties of the specimen are presented in Table 1. DW-55LSR electrode with a diameter of 1.2 mm was used for the weldment generation [9]. The chemical composition and mechanical properties of the electrode are presented in Table 2.

Table 1. Chemical composition and mechanical properties of AH32

C	Si	Mn	P	S	Ni	Cu	Mo
0.15	0.14	0.91	0.19	0.44	0.01	0.02	0.02
Yield Stress				310 MPa			
Ultimate Strength				500 MPa			

Table 2. Chemical composition and mechanical properties of DW-55LSR

C	Si	Mn	P	S	Ni
0.04	0.36	1.37	0.008	0.008	1.4
Offset Yield Stress			550 MPa		
Tensile Strength			585 MPa		

The geometric configuration and the dimensions of the T-joint are illustrated in Figs. 2 and 3, respectively.

Fig. 2. Geometric configuration of specimen

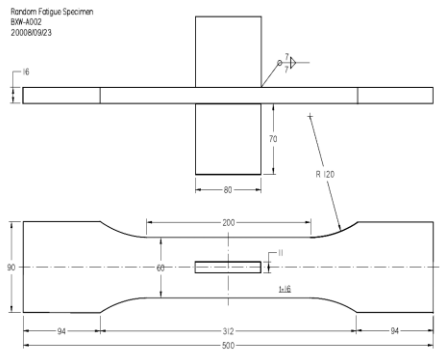

Fig. 3. Dimensional details of specimen

The welding process was arc welding with one-pass flux-cored (FCA) method. Table 3 shows the welding parameters such as electric current, voltage, welding speed, and arc efficiency.

Table 3. FCA welding conditions

Welding Condition	
Current (A)	230
Voltage (V)	27
Speed (Cm/min)	50
Arc Efficiency (%)	80

Several experimental methods are available for measuring residual stresses. They include XRD (X-ray diffraction), deep hole drilling, slicing, and magnetic methods. The XRD technique is capable of establishing these stresses in the interior of components non-destructively. The principle of stress analysis by XRD is based on measuring the angular lattice strain distributions. With the XRD method, components of strain are obtained from measurements of changes in the lattice spacing of crystals. Noyan and Cohen (1987)[10] and Cullity (1978)[11] explain in detail the complete method for measuring residual stresses. In this work, the XRD measurements of residual stresses near the weld bead are based on the following equation [3].

$$\sigma_\phi = \frac{E}{(1+\nu)\sin^2\psi}\left(\frac{d_{\phi\psi}-d_0}{d_0}\right) \tag{1}$$

where σ_ϕ is the surface residual stress; $d_{\phi\psi}$ is the interplanar spacing in the direction defined by angles ϕ and ψ, obtained from the position of diffraction peak for a given (hkl) lattice plane; d_0 is the stress-free spacing of the (hkl) lattice planes, and E and ν are Young's modulus and Poisson's ratio, respectively. The linear relationship in Eq. (1) for residual stress implies that a plot of lattice strain against $\sin^2\psi$ will be a straight line, whose gradient is a function of σ_ϕ, E and ν. The value of σ_ϕ can be calculated from the gradient of a straight line fit by the least squares method through the data points for various tilt angles. Using the double-exposure technique, the residual stresses is also calculated from the difference, $\Delta\theta$, between the two diffraction angles [3]. Using Bragg's law, Eq. (1) can be rewritten as

$$\sigma_\phi = \frac{E}{(1+\nu)}\frac{\cot\theta\Delta\theta}{\sin^2\psi} \tag{2}$$

Values of $\Delta\theta$ are plotted against $\sin^2\psi$, and the stress σ_ϕ is deduced from the gradient of the line. XRD also requires that the surface of the specimen is clean and even. Thus, residual stresses were measured after the specimen's surface was polished by chemical corrosion to ensure the reliability of measurement. Fig. 4 shows the dimensional details of the specimen used in the experiments and the position at which XRD is used to measure the residual stress. The stress measurements were made along the length direction, as shown in Fig. 4. The

specimens were symmetric so only the stresses in the right half were measured.
The measured values of the stresses at each point are shown in Table 4 and Fig. 5.

Table 4. Measured residual stresses

No.	Measured location (mm)	Residual Stress(MPa)
1	0	302
2	5	169.4
3	10	26.3
4	15	-70.0
5	20	-62.9
6	30	-31.0
7	40	1.6
8	60	-1.1
9	80	1.4
10	100	-2.0

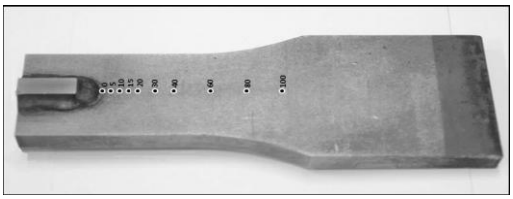

Fig. 4. Configuration of specimen and the measurement points

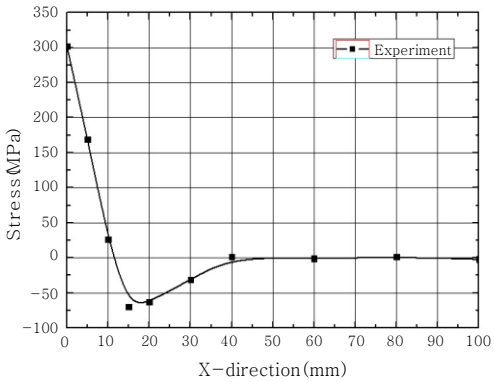

Fig. 5. Longitudinal stress along length direction

3. Computational Model of Residual Stresses

The temperature fields and the residual stresses are estimated by means of 3-D finite element method. In this study, the thermo-mechanical behavior of the weldment during welding is simulated using an coupled thermo-mechanical finite element formulation using the MSC.Marc code [12]. In the present study, the thermal analysis and the mechanical analysis were coupled and conducted in sequence. As a first step, the thermal analysis was carried out calculating the transient temperature distribution during welding. As a second step, the mechanical analysis was conducted based on the temperature field. The finite element model employed for the mechanical analysis is similar to the thermal model except for the boundary conditions. The thermal analysis was based on the heat conduction formulation with a double ellipsoidal heat source composed of a surface flux and a volumetric flux. For the analysis, the eight-node brick element was chosen.

3.1 FE Modeling

The 3-D finite element model is shown in Fig. 6 with 17,597 eight-node brick solid elements and 22,831 nodes for both the heat transfer analysis and the thermo-mechanical analyses. The eight-node hexahedral brick elements were chosen using fully-integrated Gaussian quadrature in order to avoid the hourglass mode. The Newton-Raphson method and the backward difference method were selected as the numerical schemes for the nonlinear equation and the time integration, respectively.

Contact elements were generated on the boundary surfaces of the weldment and the base metal since it is difficult to generate the nodes of the weldment on the same location of horizontal plate, and vertical plates. The finite element model also utilizes the technique of element birth and death to simulate the weld filler generation with time. The whole FE model is generated in the start, however, all elements representing filler metal are deactivated by assigning them very low stiffness to simulate the “element death” effect. Similarly, mass, specific heat, and other stiffness effects are set to zero for deactivated elements. Deactivated elements are “born” sequentially when they come under the influence of the welding torch. Similarly, its stiffness, and other attributes return to their original value when elements are born. Mechanical behaviors are computed for newly activated elements according to the current temperature. For the subsequent structural analysis, melting temperatures are set as reference temperatures (temperature at which

the thermal strain is zero) for thermal expansion coefficients of filler and base metals, respectively.

In the mechanical analysis, boundary conditions are just used to prevent rigid body motion. The boundary condition is shown in Fig. 7. Twelve points on both sides of horizontal plate were constrained in all directions.

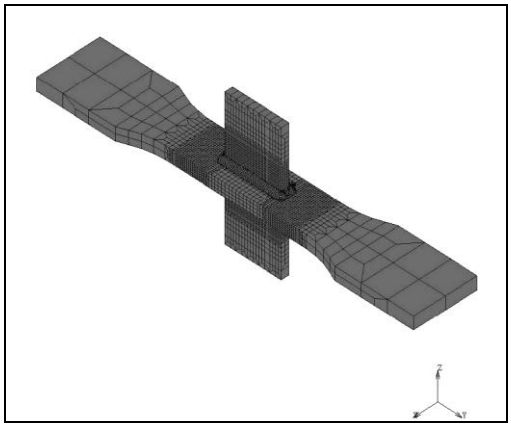

Fig. 6. Finite element mesh

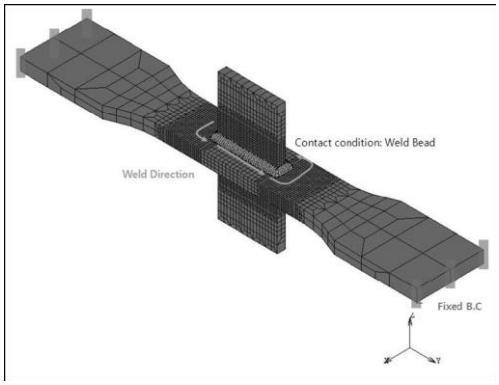

Fig. 7. Contact condition and boundary conditions applied to the specimen

3.2 Material Properties

In thermal analysis and mechanical analysis, the computations used temperature dependent thermo-physical and mechanical properties of the base metal and the filler metal. The thermo-physical properties and mechanical properties of the AH32 steel are shown in Fig. 8 and Fig. 9, respectively. The plastic hardening model was assumed to be nonlinear isotopic hardening and to follow the von Mises yield criteria and the associated flow rules. The stress-strain curves are depicted in Fig. 9. The phase transformation temperatures, the corresponding latent heats, and the way in which the latent heat was released during the phase transformations were considered in the model. Metallurgical phase transformation effects were not considered in our analysis due to the lack of a thermo-metallurgical model in MSC.Marc.

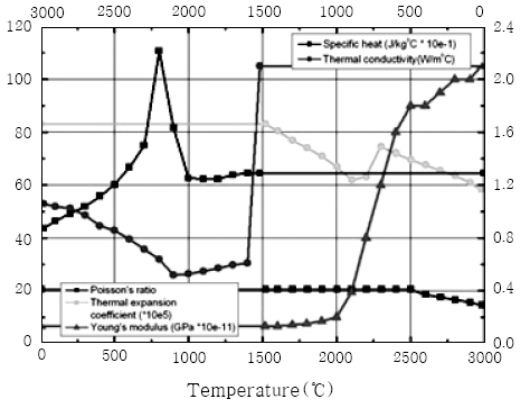

Fig. 8. Material property versus temperature

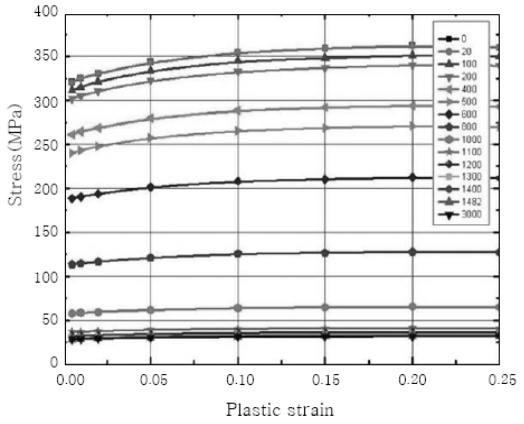

Fig. 9. Stress-plastic strain dependence on temperature

3.3 Heat source of Arc FCA Welding

The first step in the analysis of welds is to accurately determine the transient temperature field. We have used a 3-D heat diffusion finite element model to simulate heat transfer during welding. The governing energy balance equation for transient heat transfer analysis is given as follows:

$$\nabla \cdot \nabla (kT) + Q(x,y,z,t) = \rho C_p \frac{\partial T}{\partial t}(x,y,z,t) \quad (5)$$

where, k is the heat conduction coefficient, T is the temperature, Q is heat generation rate, t is the time, and (x,y,z) is the coordinates in reference system, ρ is the density of the substance, and C_p is the specific heat capacity.

According to the nature in which energy is transferred from the arc, the heat input of the FCA welding process to the weldment can be modeled by the heat flux on the surface or the heat generation distribution in the metal, or a combination of the two. In this work, the heat from the moving welding arc is applied as a volumetric heat source with a double ellipsoidal distribution proposed by Goldak et al. (1984)[13]. They proposed a 3-D double ellipsoidal heat flux model to examine the 3-D temperature, stress, and strain fields. The heat source distribution, as shown in Fig. 10, combines two different ellipses; i.e., one in the front quadrant of the heat source and the other in the rear quadrant.

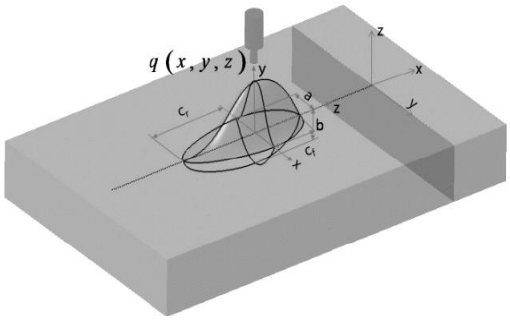

Fig. 10. Goldak's double ellipsoidal heat source

The heat flux distribution is represented by the following equation [13]:

$$Q_{f,r(x,y,z)} = \frac{6\sqrt{3} f_{fr} Q_W}{abc_{f,r}\pi\sqrt{\pi}} e^{-3x^2/a^2} e^{-3y^2/b^2} e^{-3z^2/c^2} \quad (5)$$

where $Q_W = \eta VI$ is the energy input rate determined by welding current I, voltage V, and efficiency η. f_f and f_r are the fractional factors of the heat deposited in the front and rear quadrant, as determined by $f_f + f_r = 2$. The parameters of the heat source (a, b, c_f, and c_r, as shown in Fig. 10) define the size and shape of the ellipsoidal distribution of the heat source. The welding efficiency was assumed to be 80% as proposed by Atkins et al. (2002)[14].

It must be noted that fractional values f_f and f_r should be incorporated in Eq. (5) to provide the good correspondence between the measured and calculated temperature distribution. In order to validate the heat flux model, the weld section was polished and chemically etched to reveal liquidus isotherms and HAZ isotherms. We compared the measured isotherms at a section of the specimen with corresponding simulation isotherms plotted in Fig. 11. Good agreement is found between liquidus isotherms and outer HAZ dimensions. The parameters a, b, c_f, and c_r, which were used to estimate the heat flux, were selected based on parametric trials in which the simulated HAZ was identical to that of the specimen. Table 5 summarizes the parameters of heat flux model determined by the comparison. Using the parameters, thermal analysis produced the same HAZ as that observed in the real specimen.

Table 5. Parameters for heat flux distribution

a (mm)	b (mm)	c_f (mm)	c_r (mm)
7	7	5	9

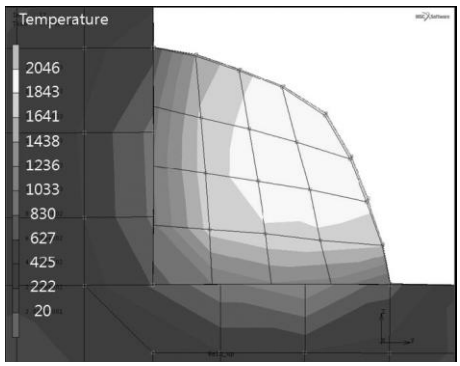

Fig. 11. Temperature distribution on the weldment.

Heat losses due to convection and radiation (q) are also taken into account in the finite element models. All surfaces of the model are assumed to lose heat by convection to the surrounding air. Heat

loss due to convection is accounted for using Newton's law:

$$q = h(T_s - T_o) \tag{6}$$

Here, h (W/m^2 ℃) is the heat convection coefficient, T_s and T_o denotes the surface temperature of the workpiece and the ambient temperature, respectively. Therefore, the convection boundary conditions were employed to account for surface heat losses due to natural convective heat transfer and Stefan-Boltzmann radiation. For a surface element contacted by flowing gas or liquid, the heat flow density q is, according to Newton's law, proportional to the difference between surface temperature T_s and gas or liquid temperature T_o through the coefficient of convective heat transfer h . In this study, a temperature-dependent heat convective coefficient is used and the ambient temperature is assumed to be 20℃ [15, 16, 17]. The heat loss due to radiation is modeled using the Stefan-Boltzmann law:

$$h = 24.1\times10^{-4}\varepsilon^r T^{1.61} \tag{7}$$

Where, ε is the emissivity (degree of blackness) of the surface of the body. A value of 0.9 was assumed for ε^r , as recommended for hot rolled steel [17].

3.4 Mechanical analysis

The same FE mesh used in thermal analysis is employed by the mechanical analysis, except for the boundary conditions. The analyses are conducted using the temperature history calculated by the thermal analysis as the input information. Temperature-dependent thermal properties such as the modulus of elasticity, yield strength, and thermal expansion coefficient are used for mechanical analyses. Given the phase transformation of steel and its effect on the welding residual stress and deformation, the total strain (ε^{total}) can be decomposed into three components as follows [18]:

$$\varepsilon^{total} = \varepsilon^e + \varepsilon^p + \varepsilon^{th} \tag{8}$$

Here, ε^e , ε^p , and ε^{th} are the elastic, plastic, and thermal strains, respectively. The elastic strain is modeled using Hooke's law with a temperature-dependent elastic modulus. The Von Mises yield surface and temperature-dependent material properties are employed to model the plastic strain.

3.5 Numerical result

The temperature distributions of points near the bead toe are shown in Fig. 12. It shows the temperature distribution, obtained by FEA, along the longitudinal direction of three nodes located at the end of the weld toe, as shown in Fig. 4. The maximum temperature around the welded toe reached 1,150 ℃. When the electrode was applied to a substrate structure, there was an immediate response consisting of a very steep temperature distribution in the vicinity of the bead generation. Subsequently, the temperature profile became smoother as the heat diffused throughout the structure.

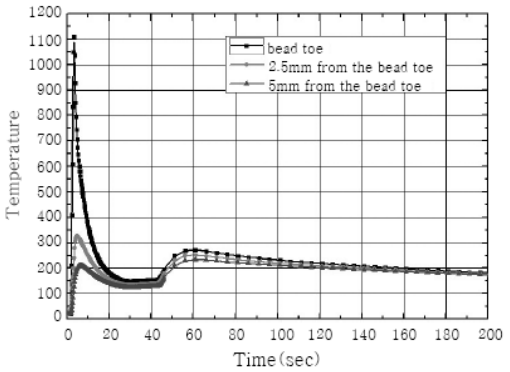

Fig. 12. Temperature histories at several points

Heat diffusion analysis showed that the plate reached a steady state temperature distribution after cooling down. The residual stresses at steady state are shown in Fig. 13. Also, to capture the residual stress distribution along the plate, three paths were defined along the x-axis as shown in Fig. 14. The longitudinal stress results were compared to the XRD measurement. The pattern of residual stresses of FEA shows good agreement with those of experiments if we consider the nonlinearity of the computational welding model. Also, to capture the residual stress distribution (longitudinal stress) along the plate, three paths (A-B, C-D, and C-E) were defined along the axes as shown in Fig. 14. Residual stresses along the length, breadth, and thickness

directions of the specimen were measured. Our results are summarized as follows:

- Fig. 15 shows the residual stresses along path A-B. A large tensile residual stress occurred near the fillet welds. In the region away from the welds, a compressive residual stress occurred. The value of the maximum tensile residual stress reached the yield stress of the material.
- Fig. 16 shows the residual stress on path C-D. Compressive residual stress was dominant because the horizontal breadth of the specimen was small.
- Fig. 17 shows the residual stresses on path C-E. We note the general phenomenon that stresses decreased along the thickness direction.

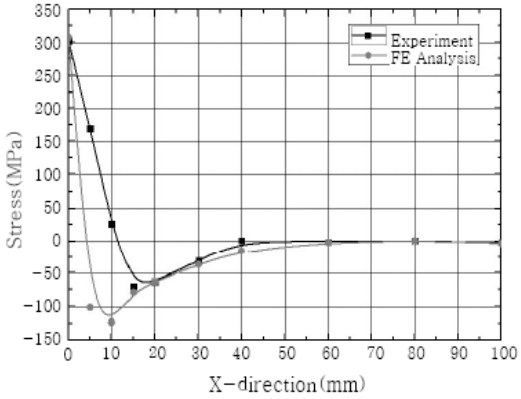

Fig. 13. Longitudinal stresses obtained by experiment and FEA

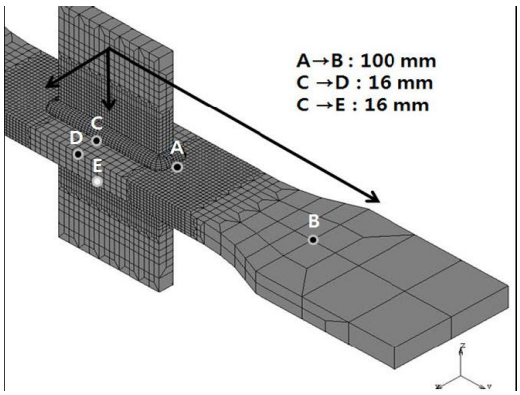

Fig. 14. Locations of measurement points and directions

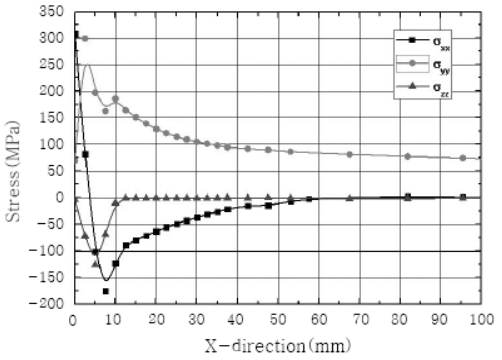

Fig. 15. Residual stress distribution along path A-B

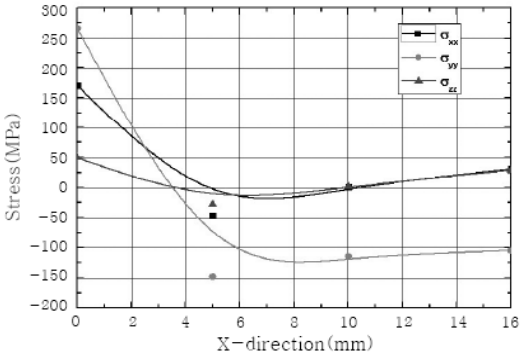

Fig. 16. Residual stress distribution along path C-D

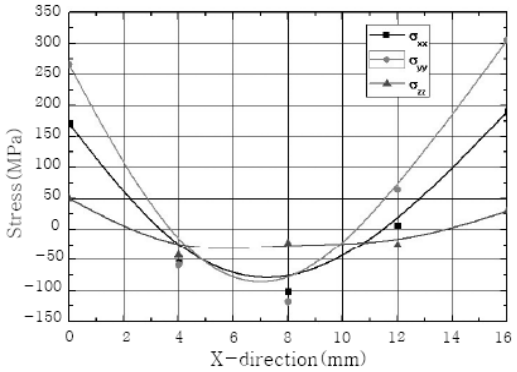

Fig. 17. Residual stress distribution along path C-E

4. Conclusion

We described the residual stress distribution in a T-joint fillet. T-joints in marine vessels frequently experience fatigue damage. We performed a 3-D

thermal elasto-plastic FEA to evaluate residual stresses in T-joint fillet welds. XRD measurement results were used to validate the FE model. We developed a finite element model for the numerical simulation of welding residual stresses in high strength carbon steel (AH32) welds. A 3-D finite element welding simulation was carried out on a one-pass FCA welded T-joint structure. The welding simulation was considered to be a coupled thermo-mechanical analysis and the element birth and death technique was employed to simulate filler metal deposition. The FEA results of the residual stress distributions of T-joint welded plates were described. The values of the longitudinal residual stresses calculated using FEA were investigated. The results obtained by the finite element method are in good agreement the experimental results.

The proposed method for welding simulation can be used in fatigue strength assessments of structures experiencing storm loads.

Acknowledgements

This work was supported by Mid-career Researcher Program through NRF grant funded by the MEST(2009-0080880) .

References

[1] Talijiat B, Radhakrishnan B, and Zacharia T, *Numerical analysis of GTA welding process with emphasis on post-solidification phase transformation effects on residual stress*, Material Science Engineering A, 246(1-2), (1998), 45–54.

[2] Barsoum Z and Barsoum I, *Residual stress effects on fatigue life of welded structures using LEFM*, Engineering Failure Analysis, 16, (2009), 449–467.

[3] Webster GA and Ezeilo AN, *Residual stress distributions and their influence on fatigue lifetimes*, International Journal of Fatigue, 23(1), (2001), 375-383.

[4] Teng TL and Chang PH, *Effect of residual stresses on fatigue crack initiation life for butt-welded joints*, Journal of Materials Processing Technology, 145(3), (2004), 325-335.

[5] Matsuoka K, *An evaluation method on fatigue crack initiation life at welded joints in steel structures*, Journal of the Society of Naval Architects of Japan, 178, (1995), 513-522.

[6] Tomita Y, Matoba M, and Kawabe H, *Fatigue crack growth behavior under random loading model simulating real encountered wave condition*, Marine Structures, 8(4), (1995), 407-422.

[7] DNV, *Fatigue Design of Offshore Steel Structures*, Recommended Practice, RP-C203, Det Norske Veritas(DNV), (2008).

[8] Chang PH and Teng TL, *Numerical and experimental investigations on the residual stresses of the butt-welded joints*, Computational Materials Science, 29(4), (2004), 511-522.

[9] Kobewelco Co. Ltd., *Kobewelco welding today*, 4th special edition, (2011); http://www.kobelco.co.jp/english/welding/files/kwt_special_low_temperature_4th_edition_Rev1.pdf

[10] Noyan IC and Cohen JB, *Residual Stress-Measurement by Diffraction and Interpretation*, Springer, New York, (1987).

[11] Cullity BD, *Elements of X-ray Diffraction (second ed.)*. Addison-Wesley Publishing Company, (1978).

[12] Barsouma Z and Lundbäckb A, *Simplified FE welding simulation of fillet welds – 3D effects on the formation residual stresses*, Engineering Failure Analysis, 16(7), (2009), 2281–2289.

[13] Goldak JA, Chakravarti AP, and Bibby M, *A new finite element model for welding heat sources*, Metallurgical Trans-actions, 15B, (1984), 299-135.

[14] Atkins G, Thiessen D, Nissley N, and Adonyi Y, *Welding Process Effects in Weldability Testing of Steels*, Welding Journal, April (2002), 61-68.

[15] Brown S and Song H, *Finite element simulation of welding of large structures*, Journal of Engineering for Industry, 114(11), (1992), 441–451.

[16] Vinokurov VA, *Welding Stresses and Distortion, The British Library*, Boston Spa, England, (1977).

[17] Rykalin RR, *Energy Sources for Welding, Houdrement Lecture*, International Institute of Welding, London, (1974).

[18] Yi HJ, Kim JY, Yoon JH, and Kang SS, *Investigations on welding residual stress and distortion in a cylinder assembly by means of a 3D*

finite element method and experiments, Journal of Mechanical Science and Technology, 25(12), (2011), 3185-3